Design of a Low-Power Direct-on-Line Synchronous Reluctance Motor Based on the Modified Natural Flux Line Curve Approach

Abramenko Valerii, Barta Jan, Lolova Iveta, Petrov Ilya, Pyrhönen Juha

DOI: 10.1109/TIA.2021.3108947

Design of a Low-Power Direct-on-Line Synchronous Reluctance Motor Based on the Modified Natural Flux Line Curve Approach

Valerii Abramenko, Jan Bárta, Iveta Lolová, Ilya Petrov, Juha Pyrhönen, *Senior Member, IEEE*

***Abstract*— A direct-on-line synchronous reluctance motor (DOLSynRM) with a rotor topology defined by the natural flux line curve approach is studied as an alternative to an induction motor using a 1.5 kW, 50 Hz synchronous reluctance motor as an example. If an induction motor stator is used, a direct squirrel cage rotor replacement by a synchronous reluctance rotor equipped with a damper winding might not guarantee a sufficient starting performance. To ensure the strong enough starting capability, the natural flux line curve approach was modified in the motor design. The proposed approach was applied in the optimization of the DOLSynRM using a genetic algorithm. The optimization results show a clear tendency in the rotor design when trying to achieve a reliable starting capability and to maximize the steady-state performance of the DOLSynRM. Both the stator design and the rotor diameter of the optimized DOLSynRM are different from those of a corresponding squirrel cage induction motor. A DOLSynRM prototype was built and tested. It showed about a 5.4%-unit higher efficiency than the original prototype IM and acceptable starting performance under the rated load condition. The starting capabilities of the motors under study are considered with different loads. The locked rotor apparent power and current stay below permissible limits in both the IM and the DOLSynRM.**

***Index Terms*— Damper winding, Direct-on-line, High efficiency, Inductance difference, Joukowsky curve, Line-start, Natural flux line curve, Saliency ratio, Starting performance, Synchronous Reluctance Motor.**

I. Introduction

DIRECT ON-LINE (DOL) synchronous reluctance motor (SynRM) is considered an attractive alternative to the traditional squirrel cage induction motor (IM) used in applications where no speed control is required [1]–[4]. Nowadays, most of the industrial applications, such as pumps, fans, conveyors, and other loads, are driven by IMs. Typically, the operating mode of these installations is nonstop (24/7) [5]. Therefore, the expense of consumed energy during the IM life cycle is, on average, 60–100 times as high as the cost of the motor itself [6]. At the same time, the international standards for the minimum energy efficiency of electrical machines are tightening [7]. These facts underline the importance of the efficiency of electrical drives in direct-on-line applications.

The potential of the DOLSynRM in achieving higher efficiency levels than with the corresponding IM is due to the absence of slip-related Joule losses in the rotor in the steady state [1], [3], [4]. When the DOLSynRM rotates synchronously, the damper winding (DW), which serves for starting the machine, experiences some Joule losses caused by winding and permeance harmonics. These losses, however, are much smaller in a properly designed DOLSynRM than those in the rotor of an IM [3]. Besides, the DOLSynRM is made of similar materials as a squirrel cage IM [4], which makes it more favorable than the DOL Permanent Magnet Synchronous Motor (PMSM) from the viewpoint of the initial investment cost. This is important when considering the payback time, which can be significant in the case of the DOLPMSM. For example, replacing a 7.5 kW IM of the IE1 efficiency class by the same-power IM of IE3 or a DOLPMSM of IE4 results in payback times of 0.5 and 2.8 years, respectively [8].

The DW in DOLSynRMs can be implemented either as a squirrel cage similar to IM rotors and by adding separate flux barriers [9]–[11] or by filling the SynRM rotor flux barriers with aluminum [1], [3], [4]. In the latter approach, the absence of additional steel ribs needed for the separation of the squirrel cage from the rotor barriers provides a smaller q-axis inductance, and therefore, a better steady-state performance [1], [2]. Moreover, in this case, a larger reluctance torque (compared with the case with a separate squirrel cage) allows easier synchronization of the DOLSynRM. It can be explained by the fact that the most critical synchronization point is close to the rated speed, where the torque generated by the rotor cage winding is getting smaller and a large enough reluctance torque is needed to pull the rotor into synchronism [1], [2], [6], [9]. Thus, a low rotor winding resistance and a large reluctance torque are desired for successful synchronization. From that point of view, direct filling of the barriers with aluminum is more favorable, as it provides a larger inductance difference between the d- and q-axes [1], [2], [12], and the rotor comprises a larger aluminum cross-sectional area resulting in a lower DW resistance.

The natural flux line curve approach was introduced in [13] (also referred to as the Joukowsky curve approach), where its advantages over the angular barrier shape were suggested (also over the round barrier shape in [14] and [15]). The higher potential of a DOLSynRM designed with the Joukowsky curve approach over an IM was shown in [3] and [4] with an example

of a 30 kW machine. The results pose a need for further study in other power ranges. Therefore, this paper focuses on the Joukowsky curve approach applied for the rotor design of a 1.5 kW, 50 Hz DOLSynRM addressing the research question related to the potential of a low-power SynRM as an alternative to an IM in DOL applications.

In the paper, certain difficulties in the design of the 1.5 kW DOLSynRM were identified. The Joukowsky curve approach was modified so that each barrier can be adjusted with its independent parameter. A genetic algorithm was used to design the DOLSynRM with a high efficiency. As a result, some general recommendations for the design of a DOLSynRM were suggested. They are: the size of the outermost barrier filled with aluminum should be relatively large; the size of the barrier closest to the physical d-axis should be adjusted (reduced) to enable easier rotor magnetization and inducing sufficient currents in the rotor winding for a successful start-up; the rotor diameter is recommended to be larger than in an IM of the same frame size, and the stator side can be adjusted to ensure the sufficient starting capability together with the highest steady-state performance.

II. Natural Flux Line Curve Approach in the Rotor Design of a DOLSynRM

This section describes the natural flux line curve approach applied for the rotor design of the 1.5 kW DOLSynRM. The design challenges are identified.

A. Concept of Natural Flux Line Curve Approach

The shape of flux barriers is one of the key factors to consider in the design of a SynRM. The barriers can have angular [6], circular [16], hyperbolic [10], or natural flux line curve shapes. In [13], it was shown that the natural flux line curve approach, where the flux barrier edges along the d-axis are aligned with the natural paths of the magnetic flux in the case of a smooth rotor, allows achieving the largest saliency and motor efficiency. Therefore, in this study, the natural flux line curve approach is used in the design of the flux barriers. There are three main parameters determining the rotor geometry: k_w, β, and α_m. The first (k_w) is a ratio of air to steel (insulation ratio) along the q-axis and expressed by equation

$$k_w = \frac{W_1 + \ldots + W_i + \ldots + W_k}{S_1 + \ldots + S_i + \ldots + S_{k+1}}, \quad (1)$$

where W_i is the width of the i^{th} flux barrier along the q-axis, S_i is the width of i^{th} flux guide along the q-axis, and k is the number of flux barriers.

The second parameter, angle β, serves for adjusting the position of the flux barriers. The angle β is a somewhat abstract concept as it determines the angle span between the q-axis and the position where the rotor slot pitch angle α_m starts to be measured. The third is an angle α_m determining the position of the end points of the rotor flux barriers. It is determined by equation

$$\alpha_m = \frac{45° - \beta}{k + 1/2}, \quad (2)$$

where k is the number of flux barriers.

The rotor slot pitch α_m is kept constant; however, when β is larger than zero, the end points of the outermost flux barrier S_k and W_k are calculated based on the distribution of magnetic voltage over the flux guides by equations provided in [13] or in [17]. In principle, only k_w and β determine the rotor geometry unambiguously in the natural flux line approach. All the equations that determine the flux barrier geometries are provided in the appendix.

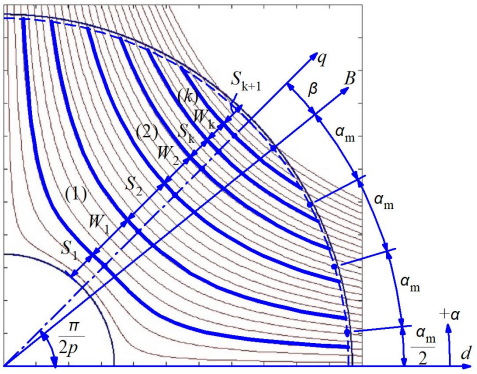

Fig. 1. Parameters defining the positions and size of flux barriers (W) and guides (S) (the subscript k indicates the number of flux barriers).

In the case of the DOLSynRM, the coefficient k_w also determines the size of the DW because k_w dictates the width of the flux barriers, which are filled with aluminum. The impact of k_w on the rotor geometry of the 1.5 kW DOLSynRM is shown in Fig. 2.

If the SynRM operates with a frequency converter, β can be efficiently adjusted to find the optimal rotor slot pitch (α_m) to minimize the torque ripple [13]. However, in a DOLSynRM, β also impacts the aluminum distribution between the barriers, Fig. 3. Besides, it can be noticed that with a larger β the outermost flux barrier more strongly disobeys the constant rotor slot pitch rule. These features make the design of a DOLSynRM different from a SynRM dedicated for operation with a frequency converter.

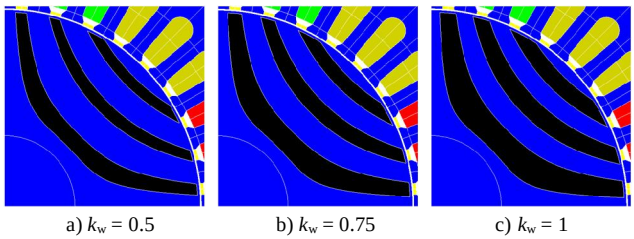

a) k_w = 0.5 b) k_w = 0.75 c) k_w = 1

Fig. 2. Impact of k_w on the rotor geometry, β=10°.

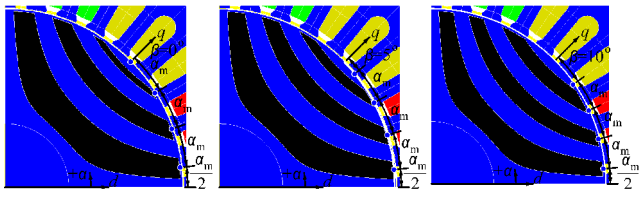

a) β = 0° b) β = 5° c) β = 10°

Fig. 3. Impact of β on the rotor geometry, k_w = 1.

B. Number of flux barriers

Usually, a SynRM with a larger number of barriers can produce a larger torque. However, according to [13], the difference between the torque capabilities with three and four

flux barriers is not significant (1.3%), and it is even less significant between four and five barriers. At the same time, the large number of barriers does not necessarily lead to a higher efficiency in the steady state as losses in the DW (caused by the stator current linkage and permeance harmonics) can grow with the number of barriers [4]. Another important factor to consider when selecting the number of barriers is the cutting/punching technology used for the manufacturing of steel sheets [6]. Such manufacturing leads to steel degradation at the edge of steel because of mechanical-cutting-caused stresses. In the present case, the 1.5 kW motor has a relatively small rotor diameter, which is not favorable for a large number of barriers regarding the negative effect of manufacturing on the electromagnetic properties of steel. Considering these aspects, the number of barriers was selected to be equal to three.

C. Design of the 1.5 kW DOLSynRM with the Natural Flux Line Curve Approach

The software Flux 12.3 was used for simulation. A 1.5 kW IM (Fig. 4) was used as a reference for the design of DOLSynRM. In the initial DOLSynRM design, the stator side was unchanged from that of the IM. The shaft was considered solid ferromagnetic.

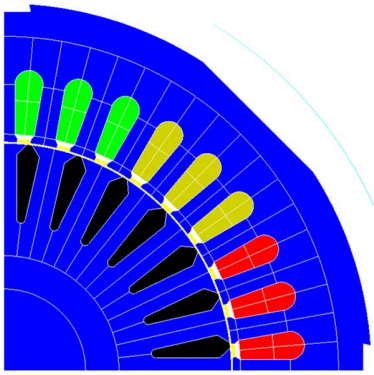

Fig. 4. 1.5 kW IM geometry used as a reference for the DOLSynRM design.

All the designed DOLSynRM versions (some of them can be seen in Fig. 3) failed in synchronization under rated load (Fig. 5). Their rotors oscillate below the rated speed lacking the reluctance and DW torques to pull into synchronism. To bring the motor closer to synchronization, it should have a small DW resistance. Large reluctance torque is desired to pull the motor into synchronism. The resistance of the DW can be reduced by increasing the flux barrier area where the aluminum is filled. On the other hand, too large a width of flux barriers can result in deterioration of the reluctance torque component. Thus, a trade-off between DW and reluctance torque components should be found to achieve a reliable starting performance.

One of the reasons for the synchronization failure of the 1.5 kW DOLSynRM is the relatively large per-unit stator resistance, which is common in low-power machines. During the start-up, the peak of the voltage drop is approx. 160 V (Fig. 5), which is about 50% of the applied peak phase voltage ($230\cdot\sqrt{2}$ V). As the voltage determines the level of flux linkage, the motor cannot be magnetized strongly enough to provide sufficient DW and reluctance torques for synchronization [18].

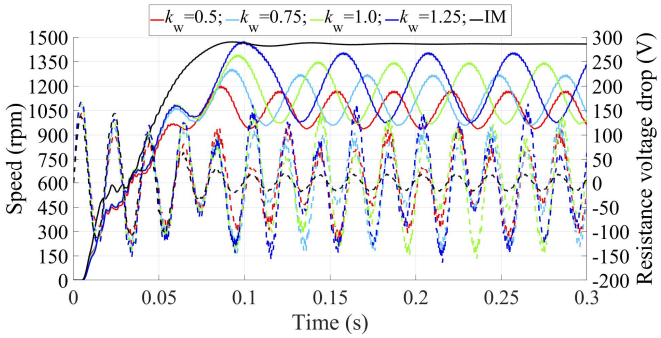

a) Impact of k_w on the DOLSynRM start-up, $\beta = 10°$

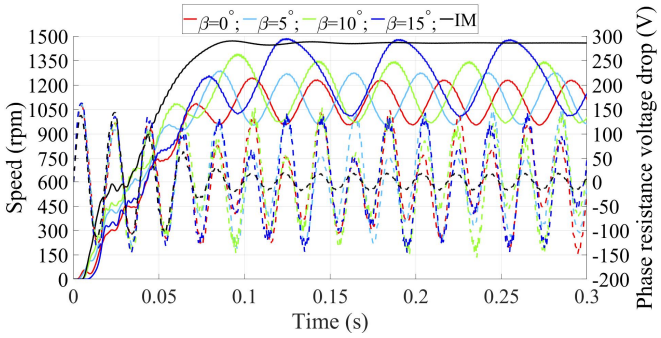

b) Impact of β on the DOLSynRM start-up, $k_w = 1$

Fig. 5. Failed start-ups (solid lines indicate speed and dashed lines the stator resistive voltage drop).

In principle, there are many other parameters which affect the DOLSynRM starting performance. For example, the magnetic circuit (which is determined by the stator and rotor geometry) affects the motor starting capability as well as the steady-state performance. The large variety of parameters poses a need to identify the ones that have the most significant impact on the starting performance.

III. Modified Natural Flux Line Curve Approach

In this work, a modification of the rotor design to provide the sufficient starting capability was implemented based on the theory originally developed in [19]. During the start-up, when the stator current linkage faces the d-axis, the magnetic flux meets a lower reluctance compared with the case with the q-axis magnetization. Therefore, the stator flux excites the aluminum much more efficiently on the d-axis than on the q-axis. At stall, the flux does not penetrate deep into the rotor even when the d-axis is magnetized because of the strong opposing DW currents. Closer to the point of the rated speed (which is the most difficult point for synchronization), the flux variation in the rotor is lower and the flux can penetrate deeper, and therefore, a much larger amount of aluminum is magnetized. In this case, the DW equivalent resistance is essentially determined by the total amount of aluminum embedded in the flux barriers. However, if the flux guides close to the physical d-axis are relatively thin (have a large reluctance), part of the flux will search other ways to flow, thus linking a smaller amount of aluminum, which deteriorates the starting performance. Similarly, the importance of the flux paths, their dependence on the number of barriers filled with aluminum, and the impact of flux paths on the rotor parameters (equivalent

resistances) was shown in [20], but no guidelines for the design were given. This may be an indication of the nature of the problem. In this work, an optimization algorithm was applied as it is not straightforward to say how the rotor must be designed to achieve a good starting property.

Simulations have shown that the thickness of flux guides, which are close to the physical d-axis, has a significant impact on the starting capability of the motor [19]. It was proven by making the flux barrier closest to the shaft thinner while keeping the same rotor diameter. In Fig. 6a, in the rotor with parameters $k_w = 1$ and $\beta = 15°$, the barrier number 1 was adjusted so that instead of $k_w = 1$, $k_w = 0.5$ was applied for only this particular barrier. This rotor synchronizes, even though it has a large speed fluctuation during the synchronization process (Fig. 6b). This shows the possibility to modify the conventional Joukowsky curve design approach when applied to a low-power DOLSynRM.

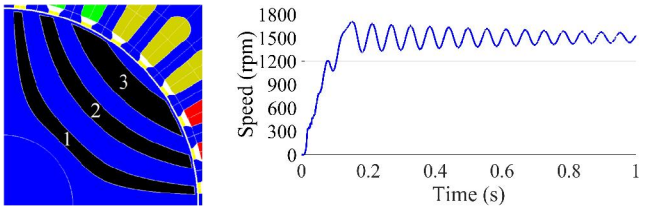

a) Rotor geometry b) Speed transient

Fig. 6. Joukowsky curve design: $k_{w1} = 0.5$, $k_{w2} = 1$, $k_{w3} = 1$, $\beta = 15°$.

Thus, to design a low-power (1.5 kW in this case) DOLSynRM by the natural flux line curve approach with a sufficient starting capability, it might be necessary to adjust the geometry of the flux barriers individually. In the proposed modified approach, the rotor geometry is determined not with the original two parameters (k_w and β), but with a k+1 number of parameters, where k is the number of flux barriers. Each barrier is described with its own k_w while β stays common for all barriers. In the case of three flux barriers, the rotor parameters are k_{w1}, k_{w2}, k_{w3}, and β. The principle of such an approach is presented in Fig. 7.

An extra minor adjustment that was added in the design of the motor under optimization is the shape of the innermost flux barrier. The barrier is assigned to have an angular shape of the contour closest to the shaft, as it is shown in Fig. 7 (adjusted design approach). It may seem to contradict the logic requiring that the flux guide next to the d-axis should be kept thick because the angular shape of the innermost barrier reduces the amount of steel in the flux guide on the d-axis. However, the reluctance of the flux guide is mostly determined by the thinnest site near the rotor periphery as it saturates first. If that thinnest site is not saturated, the steel that is deeper in the rotor does not significantly affect the magnetic permeance of the flux guide. Therefore, the barrier edge close to the physical d-axis was reshaped to increase the amount of aluminum (and also to decrease the q-axis inductance), which contributes to the starting performance of the motor. With this modification, the width of the flux guide closest to the d-axis is equal to the smallest width of the guide near the rotor periphery and can be adjusted with the parameters k_{w1} and β. Similarly, this adjustment was applied to maximize the saliency and the motor efficiency in [17] (however, only k_w and β were used to modify the rotor geometry) as a final tuning of the rotor.

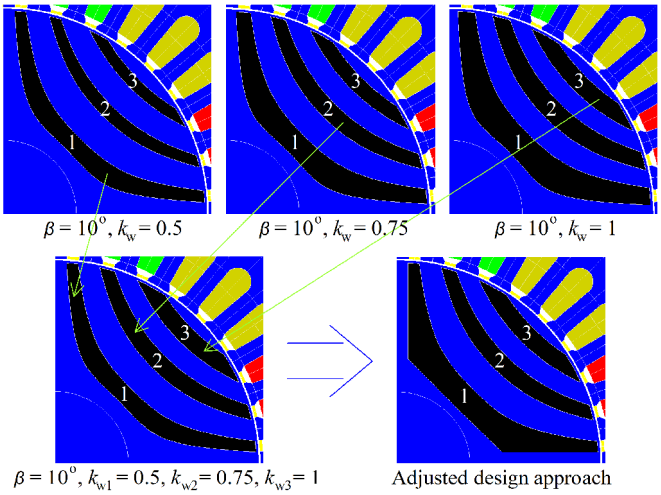

Fig. 7. Principle of the modified Joukowsky curve approach, example.

IV. Optimization with Genetic Algorithm

A. Optimization algorithm. Optimization problem formulation and boundaries

The modified natural flux line curve approach was used in the four-pole 1.5 kW DOLSynRM optimization to achieve the highest efficiency in the steady state with a sufficient starting capability. A genetic algorithm (GA) was applied as an optimization strategy [21]. The GA operates with generations that consist of individuals that represent different design modifications of the DOLSynRM. In the current case, one generation has 12 individuals, which is a relatively limited group. The selected number of individuals is explained by large computational costs for the simulation of DOL machines. Every individual has its own values of parameters, such as rotor diameter and number of winding turns. In the first generation, all the individuals are generated with randomly initialized values of parameters within the preset boundaries. The following generations consist of new individuals, which are obtained by means of selection, crossover, mutation, and elitism.

The aim of optimization is to find such motor parameters that provide the highest possible motor efficiency within given boundaries (size, materials). The objective function can be formulated as

$$\text{maximize } (\eta) = f(k_{w1}, k_{w2}, k_{w3}, \beta, D_r, N_s, h_s, b_{ds}) \quad (3)$$

subject to constraints in Table I.

The crossover rate was 0.8, the mutation rate was 0.1, and elitism ensured that two best individuals among all the previous generations always proceed to the current generation and take part in the production of the next generation.

TABLE I
BOUNDARIES OF THE OPTIMIZED PARAMETERS

Name	Lower limit	Upper limit	Values of corresponding IM
Stator slot height, h_s (mm)	10	17.5	13.65
Stator tooth width, b_{ds} (mm)	3.2	4.2	3.7
Number of turns in series in stator phase winding, N_s	144	288	210
Rotor diameter, D_r (mm)	80	95	83.5
Beta angle, β (°)	0	30	-
k_{w1}	0.5	1.5	-
k_{w2}	0.5	1.5	-
k_{w3}	0.5	1.5	-

TABLE II
APPLIED EQUIPMENT AND TIME EXPENSES

Name	Value
CPU X5690	
Frequency (GHz)	3.46
Number of cores	6
RAM (Gb)	96
HDD occupied (Gb)	458
Number of simulations run at a time	2
Simulation time step (ms)	0.5
Total time elapsed (days)	31

The rotor surface tangential ribs have a strong impact on the reluctance of the rotor. It is desired to make them as thin as possible to minimize the q-axis inductance; however, they need to be sufficiently thick to keep the rotor robust. In addition, thin ribs allow aluminum locations in barriers closer to the rotor surface, which contributes to the starting performance [4]. Therefore, the thickness of the ribs was selected minimum from the viewpoint of manufacturing capabilities, being 0.5 mm. The mechanical analysis of the rotor with a diameter of 95 mm is shown in Fig. 8. The maximum von Mises stress is below 13 MPa, while the yield strength of the steel M470-50A used in the rotor is 210 MPa, which means that 0.5 mm ribs have a large safety margin.

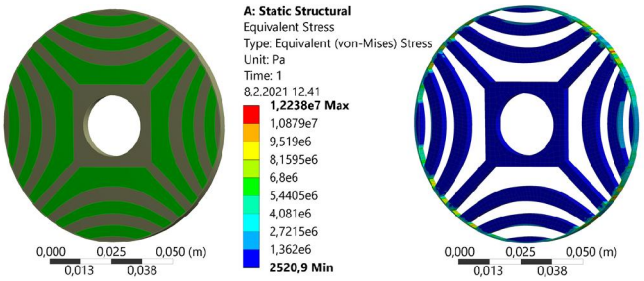

a) Simulated model b) Von Mises stresses in the rotor core

Fig. 8. Mechanical analysis of the DOLSynRM rotor. The diameter is 95 mm.

B. Simulation approach

In the case of DOLSynRM optimization, the simulation time is determined by the number of generations and by the number of individuals in each generation. In addition, the simulation of one motor can vary depending on the time of reaching the steady state. Therefore, to minimize the optimization time, a larger time step is preferable. As a rule of thumb, the minimum number of points per electrical period is 40, which was used in the optimization. Because the calculation error pertains to all individuals, comparative analysis with the selected time step should be appropriate for the optimization procedure. The equipment and time expenses for the optimization are listed in Table II.

Voltage sources were used in the simulation. The rated load torque was applied during both the start-up and the steady state. An automatic analytical calculation of the moment of inertia of the DOLSynRM rotor is complicated to implement because of the nonhomogeneous structure of the rotor. Therefore, the rotor moment of inertia was assumed to be equal to the moment of inertia of the IM rotor (estimated analytically) and was kept constant during the optimization. This assumption is acceptable because a larger amount of aluminum (which is lighter than steel) is used in the DOLSynRM rotor.

The resistivity of aluminum is another important parameter that directly impacts the starting performance. The conductivity of aluminum was determined by the range of 12–34 MS/m available from the manufacturer. In order to bring the motor closer to the synchronization point, the maximum conductivity was selected (34 MS/m). This material was also used in the prototype of the 1.5 kW IM. The temperature of the motor increases during operation, which impacts the resistivity of aluminum. According to the measurements obtained for 1.5 kW IM, the temperature in the motor was 71.5 °C after the continuous nominal load test, which should be taken into account in the simulation. The material resistivity was recalculated to be 3.5×10^{-8} Ωm based on the temperature.

C. Optimization results

The results of optimization are presented in Fig. 9. The successfully synchronizing designs are shown with blue points and nonsynchronizing designs with red points. Obviously, the motors that could not synchronize do not demonstrate high efficiency, because their speed fluctuates below the rated speed similarly as in Fig. 5.

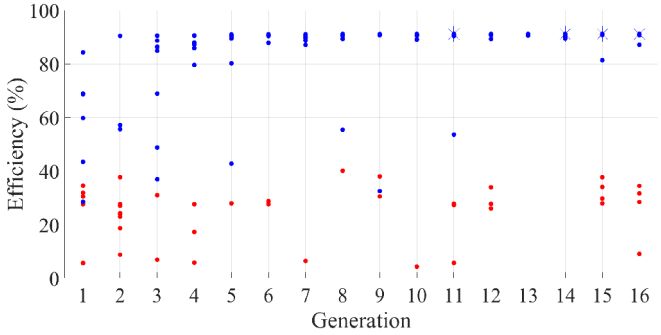

Fig. 9. Efficiency values of individuals during 16 generations with 12 individuals in each generation (red points represent failed synchronization, blue points successful synchronization).

Starting from the 11th generation, the efficiency does not grow significantly, and as the optimization has achieved saturation, it was interrupted at the 16th generation. The designs with the highest performance from the 11th and 16th generations and from the 14th and 15th generations (indicated by stars in Fig. 9) have minor differences in the optimized parameters. Therefore, only the most efficient motors from the 11th and 15th generations are considered in detail below. These selected

DOLSynRMs and the original IM were also simulated with 160 points per electrical period (instead of 40) to obtain more accurate results. The steady-state and starting performances of these motors are considered in the following section.

V. Analysis of the Optimization Results and the Main Findings Concluded

In this section, the impact of the optimal design parameters of the DOLSynRM are discussed. The starting performance is also studied. Compliance with standards with regard to a locked rotor apparent power and current is estimated.

A. Optimal geometrical parameters of DOLSynRM

The geometries, the flux density distributions, and the flux lines of the motors in the steady-state operation are presented in Fig. 10. In both the DOLSynRMs, the flux density in the stator yoke is higher than in the stator teeth, which is different from the common practice to keep the flux density in the yoke lower than in the teeth [18]. Such a result may be related to the fact that a reduction in the stator yoke results in a more significant increase in the stator slot area than the reduction in the teeth width. Large stator slots contribute to a reduction in the stator winding resistance, which is important in the case for achieving an acceptable DOLSynRM starting performance. The geometrical parameters of the motors are given in Table III. The steady-state performance data of the optimized DOLSynRMs compared with the IM are provided in Table IV.

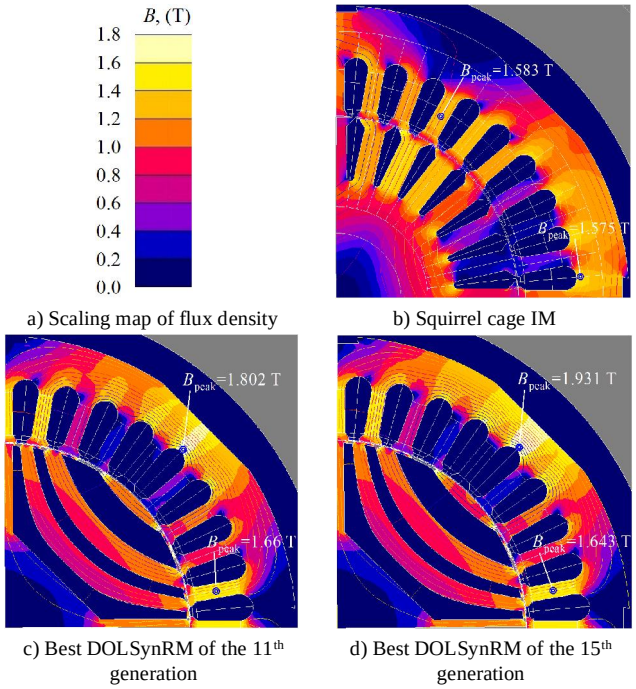

a) Scaling map of flux density

b) Squirrel cage IM

c) Best DOLSynRM of the 11th generation

d) Best DOLSynRM of the 15th generation

Fig. 10. 1.5 kW motors under study. The peak of the flux density is indicated in the stator yoke and teeth.

TABLE III
Design Parameters of the IM and the Optimized Models
(Names of the Varied Parameters in the Case of DOLSynRM Optimization Presented with Orange Background)

Name	IM	Best of 11th gen.	Best of 15th gen.
Stator slot height, h_s (mm)	13.65	14.78	14.81
Stator tooth width, b_{ds} (mm)	3.70	3.38	3.40
Number of turns in series in stator phase winding, N_s	210	234	234
Rotor diameter, D_r (mm)	83.50	85.64	86.89
Beta angle, β (°)	-	19.91	19.87
k_{w1}	-	0.71	0.86
k_{w2}	-	1.31	1.31
k_{w3}	-	0.80	0.77
Stator resistance, R_s (Ω)	3.96	3.70	3.65
Copper space factor*, k_{Cu} (%)	46.97	46.97	46.97
Stator slot cross section**, S_{slot} (mm^2)	55.4	67.6	68.8
Air-gap length, δ (mm)	0.25	0.25	0.25
Stator outer diameter, D_{se} (mm)	135	135	135
Ratio of stator inner diameter to outer diameter, D_s/D_{se}	0.62	0.64	0.65
Stack iron length, l (mm)	160	160	160

* Copper space factor is defined as a ratio of the insulated copper to the insulated slot area.

**Slot area does not include pre-slot and wedge areas. Ω

TABLE IV
Steady-State Performances of the IM and Optimized Models

Name	IM	Best of 11th gen.	Best of 15th gen.
Output power, P_{out} (W)	1512	1500	1500
Speed, n (rpm)	1457.64	1500	1500
Motor moment of inertia, J_M (kg·m^2)	0.0058	0.0058	0.0058
Load moment of inertia, J_{ext} (kg·m^2)	0.0058	0.0058	0.0058
Torque, T (Nm)	9.91	9.55	9.55
Peak-to-peak torque ripple, ΔT (Nm)	4.24	10.23	10.04
Line-to-line voltage, U_{ll} (V)	400	400	400
Stator current, I_s (A)	2.96	2.98	2.98
Magnetizing inductance, L_m (mH)	446.89	–	–
d-axis inductance, L_d (mH)	–	474.60	466.90
q-axis inductance, L_q (mH)	–	43.50	43.00
Inductance difference, L_d - L_q (mH)	0	431.20	423.90
Saliency ratio, L_d/L_q	1	10.92	10.86
Power factor, cos(φ)	0.83	0.80	0.80
Stator Joule losses, P_{CuS} (W)	103.92	98.31	97.23
Rotor Joule losses, P_{CuR} (W)	49.94	20.33	19.32
Total Iron losses, P_{Fe} (W)	52.46	52.42	53.80
Efficiency, η (%)	87.99	89.76	89.80

The results suggest that the DOLSynRM designed in the frame size of the IM should have a different stator design and rotor diameter to achieve the highest efficiency and the sufficient starting capability. The geometrical parameters of the optimal solutions found support the proposed recommendations in Section III to enhance the starting capability. The first is to keep the thickness of the innermost flux barriers limited to provide enough magnetization of the rotor for sufficient DW currents during the start-up. The second is to have a large amount of aluminum in the outermost barrier as it is linked by the largest part of flux during the start-up experiencing the largest induced back-emf, and therefore, the part of DW in the outermost flux barrier should have a small resistance to enable sufficient starting currents in the rotor. The parameter β has a strong impact on such rotor structure shaping. With a larger β, the area of the outermost barrier increases, and the thickness of the flux barriers that are close to the d-axis decreases.

According to the optimization results, the value of β should be much larger for a successful start-up in comparison with the optimal values for the steady-state performance of a SynRM controlled by a frequency converter, where β serves only as an adjusting parameter for the torque ripple minimization, and the optimal value is usually found below 10 degrees [13]. Almost all successfully synchronized motors have β larger than 10 degrees (Figs. 11 and 12). The highest efficiency, which is mostly determined by the stator winding Joule losses, is achieved with large values of β.

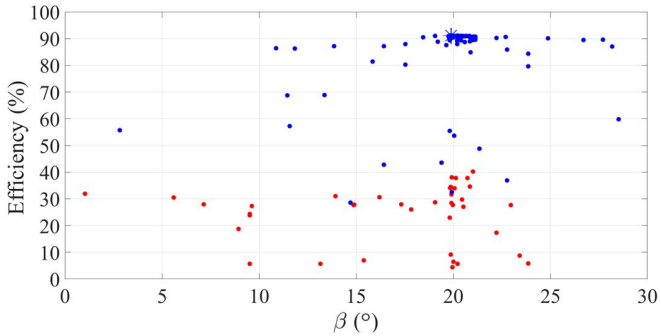

Fig. 11. Efficiency of individuals during 16 generations with 12 individuals depending on β (red points represent failed synchronization and blue points successful synchronization).

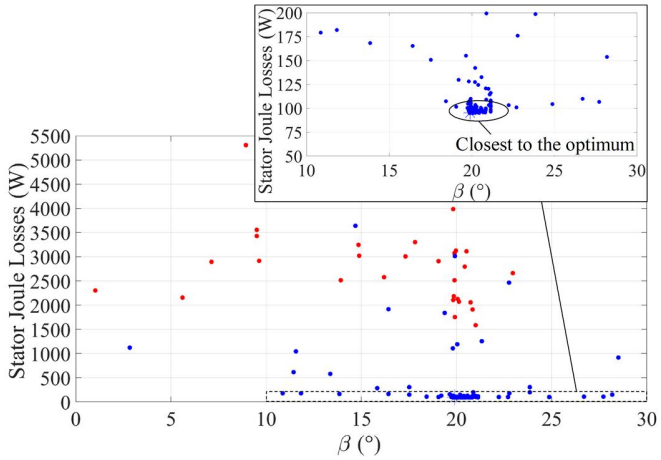

Fig. 12. Stator winding Joule losses of individuals during 16 generations with 12 individuals depending on β (red points represent failed synchronization and blue points successful synchronization).

Thus, the optimal β for the studied four-pole 1.5 kW DOLSynRM is about 20 degrees. The thin enough innermost barrier (or thick innermost flux guide) is achieved with a small k_{w1} and a large β. The size of the outermost flux barrier is determined by k_{w3} and β; however, to have a large enough area in that barrier, k_{w3} should not necessarily be larger than k_{wi} for other barriers if the value of β is relatively large (Table II).

B. Additional estimation of the starting performance

The DOLSynRM was optimized with twice the rotor moment of inertia of the IM (considered as a base value J_{init}) to make a fair comparison. All successfully synchronized DOLSynRMs are capable of achieving the synchronous speed with the total moment of inertia of $2 \cdot J_{init}$ under the rated load torque. In Fig. 13, the speed transients of the IM and the optimized DOLSynRMs are shown. However, the DOLSynRM cannot achieve the synchronous speed with the moment of inertia larger than $2 \cdot J_{init}$. As an example, the failed start-ups under rated load torque and the total moment of inertia of $2.5 \cdot J_{init}$ are also presented. The maximum moments of inertia at which DOLSynRMs could synchronize with different load torques are shown in Fig. 14. Such results mean that the optimization should be implemented considering the load for which the motor is designed. Usually, DOL motors are designed for driving pump or fan applications, which have a moment of inertia smaller than the moment of inertia of the motor. However, if a larger moment of inertia was required and it was set as a constraint of optimization, the optimized designs could differ from the obtained ones. From the viewpoint of starting capabilities, the IM is superior as it can synchronize with the moment of inertia of $20 \cdot J_{init}$; larger values were not tested in this study.

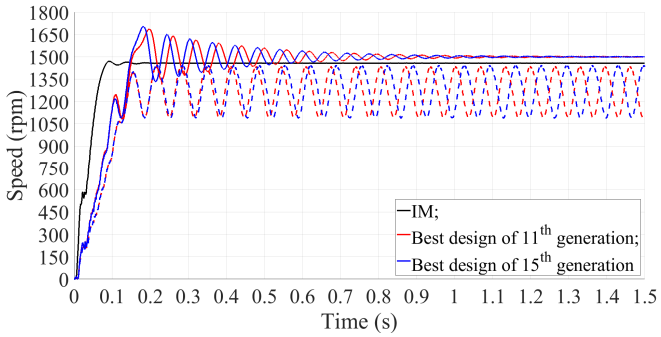

Fig. 13. Start-up speed of the IM and the optimized DOLSynRMs under the rated load torque and the moment of inertia of $2 \cdot J_{init}$ shown with solid lines (J_{init} is assumed as the moment of inertia of the IM). The dashed lines represent the speed of the DOLSynRMs under the rated load torque and the moment of inertia of $2.5 \cdot J_{init}$.

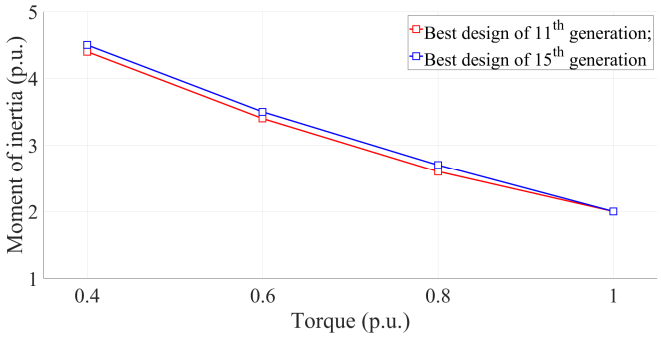

Fig. 14. Starting capability of the optimized DOLSynRMs. The moment of inertia of the IM J_{init} is assumed as a base value for the p.u. estimation of the moment of inertia.

The starting currents are naturally much larger than the steady-state rated currents. Not only they can reduce the lifetime of the motor by deteriorating the insulation material because of a high winding temperature in the case of a frequent start and stop operating mode of a motor, but also large currents may cause a significant voltage drop on the supply connected to the motor. The International European Commission has established the maximum permissible locked rotor apparent power for induction motors, which, in principle, limits the starting apparent power and current. For the motor power range from 0.4 to 6.3 kW, the permissible locked rotor apparent power can be up to 15 times the rated one according to IEC 60034-12

Edition 3.0 2016-11 [22]. Along with that, the National Electrical Manufacturers Association (NEMA) standard defines the maximum limit for the locked rotor currents directly establishing the values [23]. According to both standards, all the studied motors stay below the allowable limits. The locked rotor apparent power and current of the motors under study are listed in absolute and per unit (p.u.) values in Table V. In addition, IEC 60034-12 Edition 3.0 2016-11 suggests the equation for calculation of the locked rotor current as

$$I_\mathrm{l} = \frac{S_\mathrm{l}}{P_\mathrm{N}} \cdot \frac{P_\mathrm{N}}{\sqrt{3} \cdot U_\mathrm{N}}, \tag{4}$$

where I_l is the locked rotor current, S_l is the maximum permissible locked rotor apparent power, P_N is the rated output power, and U_N is the rated line-to-line voltage.

Following (4), the value of the maximum locked rotor current is quite close to the one of the NEMA standard (Table V). It can be seen that the locked rotor apparent power and currents are covered by a significant safe margin from the allowable limits. The waveforms of the locked rotor currents together with steady-state currents are given in Fig. 15. The waveforms for the optimized DOLSynRMs look similar, and therefore, they are given only for the best design of the 15th generation. The locked rotor currents do not have high-order harmonics because the back-EMF related to the interaction of the stator and rotor slots is absent at standstill, which is not the case in the steady state when the rotor rotates.

TABLE V
LOCKED ROTOR APPARENT POWER AND CURRENTS OF THE MOTORS UNDER STUDY

Name	Locked rotor apparent power		Locked rotor current	
	(VA)	(p.u.)	(A)	(p.u.)*
IM	17656.12	11.77	25.59	8.64
DOLSynRM 11th gen.	16849.43	11.23	24.42	8.19
DOLSynRM 15th gen.	17039.66	11.36	24.7	8.29
IEC 60034-12	22500	15	32.48	–
NEMA	–	–	32.3**	–

* The currents in p.u. values were calculated as a ratio of the RMS current at the locked rotor divided by the RMS current in the steady state.

** Calculated for 400 V as an inverse proportion to the voltage, while the original value of the current is 34 A for 380 V [23].

In the literature, IMs with the locked rotor currents exceeding 8 p.u. are reported [24]. It is natural that IMs with a higher level of efficiency have a larger locked rotor current. For example, in the official catalogue of the company WEG [25], the maximum locked rotor current of some low-power motors of premium efficiency reaches 8.9 p.u. This is explained by the fact that IMs with a higher efficiency operate at a smaller slip, which is achieved by a smaller resistance of the squirrel cage winding. However, with a low squirrel cage resistance, a stronger rotor current opposes the stator alternating flux, which, in turn, causes a larger stator current required to maintain the flux determined by the supply voltage according to equation [26]:

$$\boldsymbol{\Psi}_\mathrm{s} = \int (\boldsymbol{u}_\mathrm{s} - \boldsymbol{i}_\mathrm{s} R_\mathrm{s}) \mathrm{d}t, \tag{5}$$

where $\boldsymbol{u}_\mathrm{s}$ is the stator voltage vector, $\boldsymbol{i}_\mathrm{s}$ is the stator current vector, and R_s is the stator phase resistance.

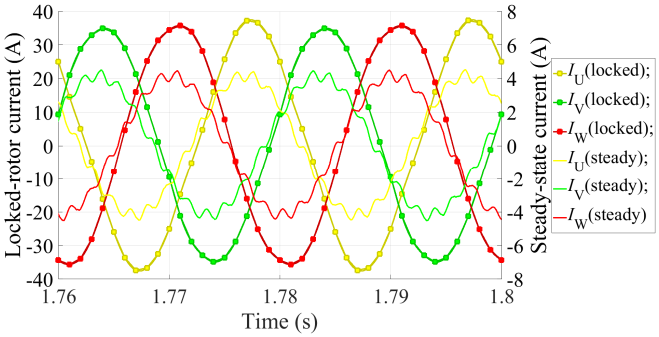

a) Induction motor

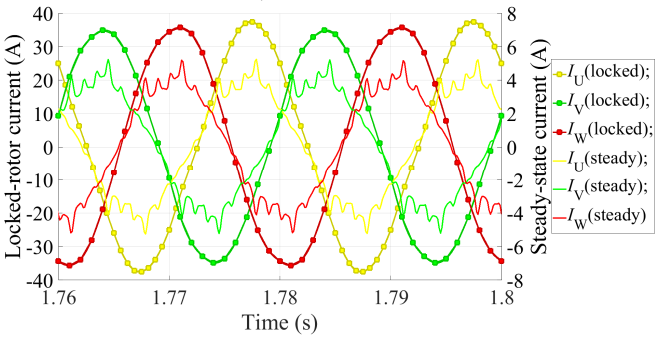

b) DOLSynRM of the 15th generation

Fig. 15. Locked rotor and steady-state currents of the simulated motors.

From this viewpoint, a DOLSynRM or a DOLPMSM can be a more advantageous solution than an IM, as they operate synchronously, and DW is required only for the starting, while in the steady state its impact on efficiency is not so significant as in an IM. Thus, to reduce locked rotor currents in a DOLSynRM or a DOLPMSM, the DW resistance can be increased until it starts to compromise the starting capabilities. However, a low DW resistance is desired for a stronger starting capability of the DOLSynRM as the most challenging starting point is near the rated speed, which was shown in the present study (Fig. 5) and also, e.g., in [1], [2].

VI. EXPERIMENTAL RESULTS

A prototype of the 1.5 kW DOLSynRM was manufactured and tested in the laboratory. The prototype has some differences compared with the optimized models. The differences were related to the stator manufacturing. The height of teeth had to be decreased and the thickness of teeth had to be increased to avoid bending of the teeth in the process of manufacturing by punching. The number of turns was also slightly adjusted. The rotor parameters of the prototype correspond to the best optimized design from the 15th generation. The prototyped motor was simulated and showed the performance very close to the performance of the DOLSynRM in Table IV, having an efficiency of 89.49%. In Table VI, the parameters of the IM and the DOLSynRM prototypes are given.

TABLE VI
DESIGN PARAMETERS OF THE MANUFACTURED IM AND DOLSYNRM
(NAMES OF THE OPTIMIZED PARAMETERS IN THE CASE OF DOLSYNRM PRESENTED WITH ORANGE BACKGROUND)

Name	IM	DOLSynRM
Stator slot height, h_s (mm)	13.65	13.68
Stator tooth width, b_{ds} (mm)	3.70	3.77
Number of turns in series in stator phase winding, N_s	210	210
Rotor diameter, D_r (mm)	83.5	85.5
Beta angle, β (°)	-	19.87
k_{w1}	-	0.86
k_{w2}	-	1.31
k_{w3}	-	0.77
Stator resistance, R_s (Ω)	3.78	3.40
Copper space factor*, k_{Cu} (%)	47.0	50.6
Air-gap length, δ (mm)	0.275	0.25
Stator outer diameter, D_{se} (mm)	135	135
Stack iron length, l (mm)	160	160

* Copper space factor is defined as a ratio of the insulated copper to the insulated slot area.

The amount of active material and the corresponding relative costs were estimated. The results are listed in Table VII. It can be seen that the total material expenses for the IM and the DOLSynRM are quite close to each other, being negligible when compared with the actual prices of the motors, where the manufacturing costs are included and amount to hundreds of US$.

TABLE VII
ACTIVE MATERIALS OF IM AND DOLSYNRM PROTOTYPES AND COSTS

Name	IM		DOLSynRM	
	Mass (kg)	Cost (US$)*	Mass (kg)	Cost (US$)*
Stator winding	0.72	7.22	0.81	8.12
Stator steel**	7.91	1.68	7.52	1.59
Rotor steel**	4.49	0.95	4.24	0.9
Rotor cage***	0.98	2.42	1.09	2.71
Total costs	14.1	12.27	13.66	12.32

* The prices price per kilogram for materials were taken from [27].
** The assumed mass densities: M470-50A 7700 kg/m^3 [28]. In the calculation, it was assumed that the shaft is of the same material as the rotor.
*** The end ring length of IM is 20 mm. With the DOLSynRM, it is 15 mm, which is related to the manufacturing constraints. The assumed aluminum mass density is 2700 kg/m^3.

The rotor and stator parts of the motor in the manufacturing stage are shown in Fig. 16. The rotor aluminum damper winding was manufactured by die casting. The laminated stator sheets were stacked together with a hydraulic press and iron clamps were mechanically added (key-fitted stator). The scheme of the test bench is shown in Fig. 17, and in the capture, the elements of the test bench are indicated. As a power source, an AC Power Source 5kVA (California Instruments 5001IX) was used, which provided sinusoidal input voltage for the DOLSynRM. A synchronous motor (SM) served as a load machine. The main elements of the test bench are shown in Fig. 18. In the sections below, the steady-state and starting performances of the prototyped motors are considered.

a) Rotor core before die casting

b) Premanufactured stack of the key-fitted stator

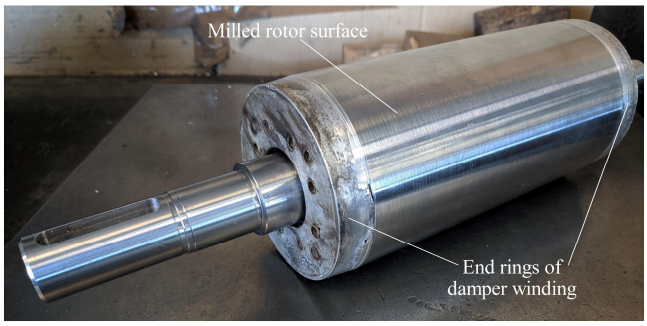

c) Completed milled rotor

Fig. 16. Motor parts of the 1.5 kW DOLSynRM during manufacturing.

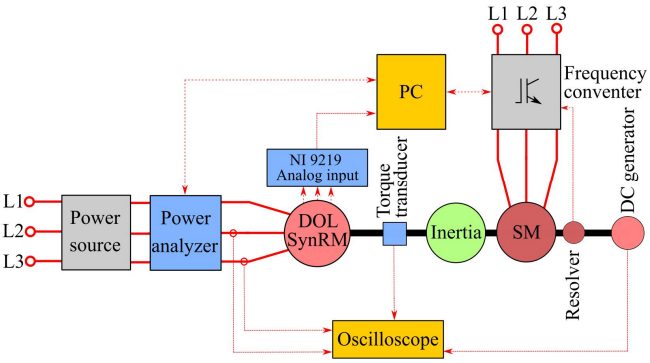

Fig. 17. Scheme of the test bench. A 5kVA AC power source supplies the DOLSynRM. A power analyzer measures the input voltage and current and sends the signals to the personal computer (PC). The PC also controls the frequency converter, which controls the synchronous machine that operates as a load in the test bench. A torque transducer and a DC generator as a tachometer provide the output torque and speed of the DOLSynRM to an oscilloscope.

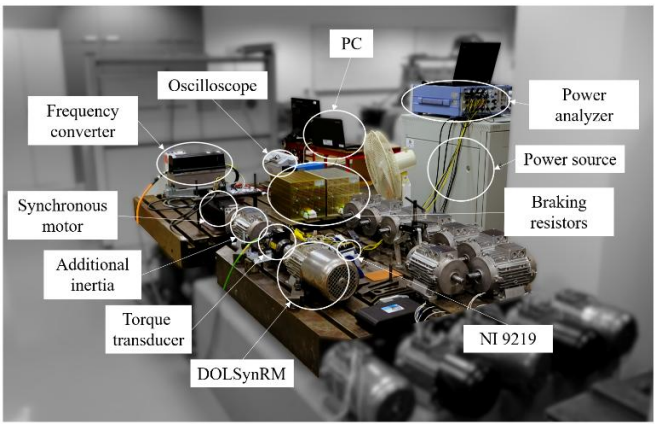

Fig. 18. Test bench for measurements.

A. *Steady-state performances of the motors prototyped*

The measured results compared with the performance of original IM prototype in the steady state are listed in Table VIII.

TABLE VIII
STEADY-STATE PERFORMANCES OF THE MANUFACTURED 1.5 KW IM AND DOLSYNRM

Name	IM	DOLSynRM
Input power, P_{in} (W)	1783.5	1710.6
Output power, P_{out} (W)	1468.14	1500
Speed, n (rpm)	1445.3	1500
Motor moment of inertia, J_M (kg·m^2)	0.0058	0.0046
Load moment of inertia, J_{ext} (kg·m^2)	0.0272	0.0272
Torque, T (Nm)	9.70	9.55
Line-to-line voltage*, U_{ll} (V)	400	400
Stator current, I_s (A)	3.59	3.62
Stator winding resistance after load test, (Ω)	3.69	3.40
Power factor, cos(φ)	0.72	0.68
Stator Joule losses, P_{CuS} (W)	144.11	133.70
Rotor Joule losses, P_{AIR} (W)	57.23	-
Total iron losses, P_{Fe} (W)	71.02	70.21**
Windage and friction losses, (W)	11.88	12
Additional losses, (W)	31.16	-
Efficiency, η (%)	82.32	87.69

*The connection type is star.
**Iron losses in the DOLSynRM at no-load may differ from iron losses in the steady state.

The mismatch between the measured and simulated results is explained as follows. The IM was simulated with the physical air-gap length of 0.25 mm instead of 0.275 mm for equitable comparison with the simulated DOLSynRM. The air-gap length of 0.25 mm is the minimum from the manufacturing point of view, and it was selected to minimize the stator winding Joule losses in the DOLSynRM. Even though with a larger air gap the iron losses should be smaller, the degradation of steel as a result of manufacturing by punching/cutting increases the measured iron losses. In addition, the degraded steel results in a magnetically larger equivalent air-gap length. There are many studies showing the dependence of the deteriorated steel area on such factors as the magnetic material, type of cutting blade, cutting speed, and methods applied [6]. The studies indicate the damaged area to be from 165 μm [29] up to several mm [30]. Low-power machines are especially sensitive to this phenomenon as they usually have a small size. It is obvious that in machines of small size, the ratio of steel with deteriorated properties to the total steel applied in the machine is larger compared with the cases with motors of larger size. This phenomenon can at least partially explain the difference between the estimated and the measured stator and rotor Joule losses. Windage and additional losses make the efficiency of the IM prototype significantly lower compared with the simulated one.

The difference between the simulated and measured losses of the DOLSynRM is more complex to explain. The measured iron losses at no-load may not be the same as in the steady state under load, because in the steady state the q-axis current also impacts the d-axis inductance by saturating the rotor ribs (cross-saturation effect), which should require less d-axis current for magnetization. Therefore, the loss separation in a DOLSynRM should differ from the case of an IM and needs an additional study, which is beyond the scope of this paper. Nevertheless, the measured efficiency at the rated operating point is straightforward and sufficient for a comparative analysis of the machines. The DOLSynRM exceeds the efficiency of the IM by almost 5.4%-units, which proves the potential of the SynRM to be a high-efficiency alternative to an IM in direct-on-line applications of low power.

B. *Stating performances of the motors prototyped*

The prototype of the DOLSynRM was measured at the rated load torque with a moment of inertia of 0.0272 kg·m^2, which is almost 2.34 times as large as the maximum load inertia at which the simulated DOLSynRMs are capable of synchronizing. Such a mismatch in the starting capabilities can be partially explained by the lower resistance of the prototype compared with those of the simulated DOLSynRMs, which is significantly caused by a larger copper space factor than the one assumed in the simulations. In addition, the starting of the DOLSynRM was implemented with a "cold" winding, which has a resistance of 2.88 Ω instead of 3.4 Ω specified in Table VI. Similarly, the damper winding resistivity of the "cold" rotor is supposed to be 2.94×10^{-8} Ωm (or conductivity of 34 MS/m), while in the simulation it was assumed to be 3.5×10^{-8} Ωm, which corresponds to the temperature in the rated operating conditions. The prototyped motor was additionally simulated with a total inertia of $5\cdot J_{init}$ assuming "cold" rotor and stator resistances, and the motor synchronized reliably. For the induction motor, the resistivity of the "cold" squirrel cage should also be 2.94×10^{-8} Ω, and the stator winding resistance is 3.13 Ω, which, however, does not affect the starting as much as with the DOLSynRM.

The locked rotor apparent power and current of the IM and the DOLSynRM were measured and are listed in Table IX. As the simulations show, the motors perform well below the permissible current limits in experimental tests. The measured locked rotor currents together with steady-state currents are shown in Fig. 19. To avoid overheating of the motors, the locked rotor current was measured at 43% of the rated voltage, and the results were then multiplied by the coefficient of 1/0.43 corresponding to the rated voltage. Only two phases were measured. It can be seen that the peak and shape of the current waveform are comparable with the simulated ones shown in Fig. 15.

TABLE IX
LOCKED ROTOR APPARENT POWER AND CURRENTS OF THE MANUFACTURED IM AND DOLSYNRM

Name	IM	DOLSynRM	Permissible limit
Locked rotor apparent power (VA)	17877.9	17498.4	22500
Locked rotor current (A)	25.91	25.36	32.48 or 32.3

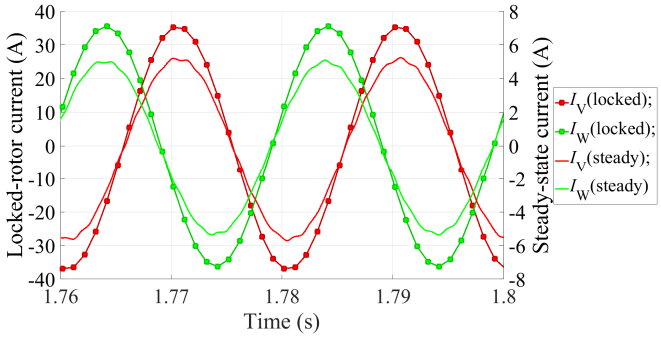

a) Induction motor

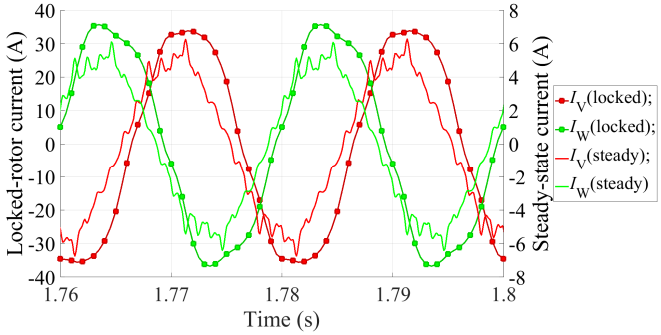

a) DOLSynRM

Fig. 19. Locked rotor and steady-state currents of the prototyped motors.

VII. Conclusion

A 1.5 kW DOLSynRM designed with the natural flux line curve (Joukowsky curve) approach as an alternative to a 1.5 kW IM and the related start-up challenges were studied. The DOLSynRM may fail to synchronize because of insufficient rotor magnetization that induces the starting currents in the damper winding. The lack of magnetization is caused by a certain rotor structure (typical Joukowsky curve approach [13]), which prevents proper rotor magnetization [19], and by a significant voltage drop (up to 50% in this case) in the stator winding resistance during the start-up transient. In addition, the aluminum distribution in the rotor determined by the flux barriers is of high importance for reaching synchronism.

The paper proposes a modified natural flux line curve (or Joukowsky curve) approach, where the thickness of each barrier is defined by its own parameter: k_{w1}, …, k_{wk}, where k is the number of barriers. The approach was applied in the optimization of a 1.5 kW DOLSynRM using a genetic algorithm. According to the results, the thickness of the innermost flux barrier should be limited (having a relatively small k_{w1}) to ensure proper rotor magnetizing, and thus, inducing sufficient starting currents in the damper winding. The optimum of the β angle, which defines the position of the barriers, should be larger in a DOLSynRM than the optimal β in a SynRM supplied by a frequency converter. In a DOLSynRM, an increase in β results in a larger outermost barrier thickness and correspondingly, its larger aluminum amount, which is more important for the start-up capability than the aluminum in other barriers. In addition, the design of the DOLSynRM stator should differ from the one of an IM having a larger inner diameter and a lower winding resistance, where the latter is achieved by adjusting the slot area and the number of turns.

Prototypes of both the IM and the DOLSynRM were built and tested. The simulation results were supported by measurements. The DOLSynRM showed a much higher efficiency (5.4%-units) and a slightly lower power factor (0.04) compared with the competing IM.

The starting capabilities of the optimized DOLSynRM and IM were studied. The IM was found superior, being capable of starting at the rated torque with the moment of inertia at least 20 times its own inertia. The DOLSynRM could only handle a load for which it was optimized. In this case, the rated torque with the double moment of inertia of the IM rotor was applied. The locked rotor (starting) apparent power or current were also considered. The simulated and measured data were similar. According to the IEC and NEMA standards, the motors under study stay below permissible limits, which was proven by experiments with the prototypes.

Appendix

This appendix provides a complete mathematical description of the rotor flux barriers with the following equations. First, the insulation ratio k_w and angle β are selected. Based on these parameters, the total width of the flux guides along the q-axis, the total width of the flux barriers along the q-axis, and the rotor slot pitch are calculated by (6), (7), and (8), respectively:

$$\sum_{h=1}^{k+1} S_h = \frac{\left(\frac{D_r}{2} - \frac{D_{shaft}}{2}\right)}{1+k_w}, \tag{6}$$

where D is the rotor diameter, and D_{shaft} is the shaft diameter;

$$\sum_{h=1}^{k} W_h = \frac{\left(\frac{D_r}{2} - \frac{D_{shaft}}{2}\right)}{1+\frac{1}{k_w}}, \tag{7}$$

$$\alpha_m = \frac{\frac{\pi}{2p} - \beta}{k+\frac{1}{2}}, \tag{8}$$

where k is the number of flux barriers, and k_w is the insulation ratio.

Then, the per-unit magnetic voltage $U_{md,h}$ applied over each flux guide when the maximum of the magnetic voltage distribution applied to the rotor is aligned with the d-axis should be calculated as

$$\begin{cases} U_{md,h} = \dfrac{\int_{\frac{2h-3}{2}\alpha_m}^{\frac{2h-1}{2}\alpha_m} \cos(p\alpha)\,d\alpha}{\alpha_m}, \text{ where } h = 1, \ldots, k \\ U_{md,h} = \dfrac{\int_{\frac{2h-1}{2}\alpha_m}^{\frac{\pi}{2p}} \cos(p\alpha)\,d\alpha}{\alpha_m+\beta}, \text{ where } h = k+1. \end{cases} \tag{9}$$

Based on the obtained voltages, the width of each individual flux guide is calculated by (6) and by

$$\frac{2S_1}{S_2} = \frac{U_{md,1}}{U_{md,2}} \;\&\; \frac{S_h}{S_{h+1}} = \frac{U_{md,h}}{U_{md,\ h+1}}, \tag{10}$$

where $h = 2, \ldots, k$.

Then, the per-unit magnetic voltage $U_{mq,h}$ applied over each flux guide when the maximum of the magnetic voltage

distribution applied to the rotor is aligned with the q-axis should be calculated as

$$\begin{cases} U_{\mathrm{mq},1} = 0, \\ U_{\mathrm{mq},h} = \dfrac{\int_{\frac{2h-3}{2}\alpha_\mathrm{m}}^{\frac{2h-1}{2}\alpha_\mathrm{m}} \sin(p\alpha)\mathrm{d}\alpha}{\alpha_\mathrm{m}}, \text{where } h = 2, \ldots, k \\ U_{\mathrm{mq},h} = \dfrac{\int_{\frac{2h-1}{2}\alpha_\mathrm{m}}^{\frac{\pi}{2p}} \sin(p\alpha)\mathrm{d}\alpha}{\alpha_\mathrm{m}+\beta}, \text{where } h = k+1. \end{cases} \quad (11)$$

The width of the flux barriers is determined by the difference between the average per-unit magnetic voltages $U_{\mathrm{mq},h}$, which is expressed as follows

$$\begin{cases} \Delta U_{\mathrm{mq},1} = U_{\mathrm{mq},2} - U_{\mathrm{mq},1} \\ \Delta U_{\mathrm{mq},h-1} = U_{\mathrm{mq},h} - U_{\mathrm{mq},h-1}, \text{where } h = 3, \ldots, k+1. \end{cases} \quad (12)$$

The width of the flux barriers is calculated by (7) and

$$\frac{W_h}{W_{h+1}} = \left(\frac{U_{\mathrm{mq},h}}{U_{\mathrm{mq},h+1}}\right)^2, \text{where } h = 1, \ldots, k-1. \quad (13)$$

Each flux barrier edge aligned with the d-axis flux is determined by the Joukowsky equation

$$r(\theta) = \frac{D_\mathrm{shaft}}{2}\sqrt[p]{\frac{C+\sqrt{C^2+4\cdot\sin^2(p\theta)}}{2\cdot\sin(p\theta)}}, \quad (14)$$

where p is the number of pole pairs, and C is a constant that depends on the point coordinates through which the curve of the flux barrier edge is passing.

Basically, $r(\theta)$ describes the flux lines inside a solid rotor.

Each flux barrier has two edges (lower and upper), and therefore, (11) should be applied twice for the determination of each flux barrier. The coefficient C is calculated based on the values of $r(\theta)$ along the q-axis; e.g., in the case of a four-pole motor, $r_1(45°) = D_\mathrm{shaft}/2 + S_1$, $r_2(45°) = D_\mathrm{shaft}/2 + S_1 + W_1$, and so on. In the case of three flux barriers, $r_1(45°) \ldots r_6(45°)$ can be calculated correspondingly, and based on the obtained values, the coefficients $C_1 \ldots C_6$ can be determined. These coefficients stay constant for every point that belongs to a certain line (describing a barrier edge), at all values of θ. The minimum and maximum values of θ are determined by the radius that limits the flux barrier on the circumference.

REFERENCES

[1] M. Gamba, G. Pellegrino, A. Vagati and F. Villata, "Design of a line-start synchronous reluctance motor," in *International Electric Machines & Drives Conference*, Chicago, 2013.

[2] M. Gamba, E. Armando, G. Pellegrino, A. Vagati, B. Janjic and J. Schaab, "Line-start synchronous reluctance motors: Design guidelines and testing via active inertia emulation," in *IEEE Energy Conversion Congress and Exposition (ECCE)*, Montreal, 2015.

[3] V. Abramenko, I. Petrov and J. Pyrhönen, "Analysis of damper winding designs for direct-on-line synchronous reluctance motor," in *43rd Annual Conference of the IEEE Industrial Electronics Society (IECON)*, Beijing, 2017.

[4] V. Abramenko, I. Petrov, J. Pyrhönen and L. Aarniovuori, "Design Aspects of Direct-on-Line Synchronous Reluctance Motors," in *XIII International Conference on Electrical Machines (ICEM)*, Alexandroupoli, 2018.

[5] I. Petrov, Y. Liu, V. Abramenko, P. Lindh and J. Pyrhönen, "Direct-on-line-start permanent-magnet-assisted synchronous reluctance machine with ferrite magnets," in *43rd Annual Conference of the IEEE Industrial Electronics Society (IECON)*, Beijing, 2017.

[6] H.-C. Liu and J. Lee, "Optimum Design of an IE4 Line-Start Synchronous Reluctance Motor Considering Manufacturing Process Loss Effect," *Transactions on Industrial Electronics*, vol. 65, no. 4, pp. 3104 - 3114, 2017.

[7] A. T. d. Almeida, F. J. T. E. Ferreira and G. Baoming, "Beyond Induction Motors—Technology Trends to Move Up Efficiency," *IEEE Transactions on Industry Applications*, vol. 50, no. 3, pp. 2103 - 2114, 2014.

[8] I. Boldea and L. Tutelea, Reluctance Electric Machines, Boca Raton: Taylor & Francis Group, 2019.

[9] Y. Hu, B. Chen, Y. Xiao, J. Shi and L. Li, "Study on the Influence of Design and Optimization of Rotor Bars on Parameters of a Line-Start Synchronous Reluctance Motor," *IEEE Transactions on Industry Applications* , vol. 56, no. 2, pp. 1368 - 1376, 2020.

[10] A. Kersten, Y. Liu, D. Pehrman and T. Thiringer, "Rotor Design of Line-Start Synchronous Reluctance Machine With Round Bars," *IEEE Transactions on Industry Applications*, vol. 55, no. 4, pp. 3685 - 3696, 2019.

[11] H. Nam, S. Park, G. Kang, J. Hong, J. Eom and T. Jung, "Design to improve starting performance of line-start synchronous reluctance motor for household appliances," in *Conference Record of the 2004 IEEE Industry Applications Conference, 2004. 39th IAS Annual Meeting.*, Seattle, 2004 .

[12] A. Takahashi, S. Kikuchi, H. Mikami, K. Ide and A. Binder, "Reluctance Torque Utility for Line-Starting Permanent Magnet Motors," *IEEE Transactions on Energy Conversion* , vol. 28, no. 4, pp. 805 - 814, 2013.

[13] R. R. Moghaddam, Synchronous Reluctance Machine (SynRM) in Variable Speed Drives (VSD) Applications, Doctoral thesis, Stockholm: KTH Royal Institute of Technology, 2011.

[14] C. Oprea, A. Dziechciarz and C. Martis, "Comparative analysis of different synchronous reluctance motor topologies," in *IEEE 15th International Conference on Environment and Electrical Engineering (EEEIC)*, Rome, 2015.

[15] A. Dziechciarz and C. Martis, "New shape of rotor flux barriers in synchronous reluctance machines based on Zhukovski curves," in *9th International Symposium on Advanced Topics in Electrical Engineering (ATEE)*, Bucharest, 2015.

[16] S. Stipetic, D. Zarko and N. Cavar, "Design Methodology for Series of IE4/IE5 Synchronous Reluctance Motors Based on Radial Scaling," in *XIII International Conference on Electrical Machines (ICEM)*, Alexandroupoli, 2018.

[17] R. R. Moghaddam, Synchronous Reluctance Machine, Stockholm: KTH Royal Institute of Technology, 2007.

[18] J. Pyrhönen, T. Jokinen and V. Hrabovcova, Design of Rotating Electrical Machines, 2nd edition, West Sussex PO22 9NQ UK: John Wiley & Sons Ltd, 2013.

[19] V. Abramenko, I. Petrov and J. Pyrhönen, "Design of Low-Power Direct-on-Line Synchronous Reluctance Motors Based on Modified Natural-FluxLine-Curve Approach," in *2020 International Conference on Electrical Machines (ICEM)*, Gothenburg, 2020.

[20] S. T. Boroujeni, M. Haghparast and N. Bianchi, "Optimization of Flux Barriers of Line-start Synchronous Reluctance Motors for Transient- and Steady-state Operation," *Electric Power Components and Systems*, vol. 43, no. 5, pp. 594-606, 2015.

[21] A. R. Parkinson, R. J. Balling and J. D. Hedengren, Optimization Methods for Engineering Design: Applications and Theory, Provo: Brigham Young University, 2013.

[22] IEC 60034-12:2016. Rotating electrical machines - Part 12: Starting performance of single-speed three-phase cage induction motors., International European Commission, 2016.

[23] NEMA Standards Publication MG 1-2009, Rosslyn, Virginia: National Electrical Manufacturers Association, 2009.

[24] A. T. D. Almeida, F. J. T. E. Ferreira and A. Q. Duarte, "Technical and Economical Considerations on Super High-Efficiency Three-Phase Motors," *IEEE Transactions on Industry Applications*, vol. 50, no. 2, pp. 1274 - 1285, 2014.

[25] WEG, "W22 Three-Phase Electric Motor," [Online]. Available: https://static.weg.net/medias/downloadcenter/h7a/hdd/WEG-w22-three-phase-electric-motor-50029265-brochure-english-web.pdf. [Accessed 2021 June 2021].

[26] J. Pyrhonen, V. Hrabovcova and R. S. Semken, Electrical Machine Drives Control: An Introduction, Chichester, West Sussex, UK: John Wiley & Sons, 2016.

[27] "Daily Metal Prices," [Online]. Available: https://www.dailymetalprice.com/metalpricecharts.php. [Accessed 15 June 2021].

[28] "DIN EN 10106. Cold rolled non-oriented electrical steel strip and sheet delivered in the fully processed state," European Standards, March 2016. [Online]. Available: https://www.en-standard.eu/din-en-10106-cold-rolled-non-oriented-electrical-steel-strip-and-sheet-delivered-in-the-fully-processed-state/. [Accessed 15 June 2021].

[29] A. Saleem, Effect of Manufacturing on Microstructure and Magnetic Properties of Non-Oriented Electrical Steel, Montreal: McGill University, 2017.

[30] A. J. M. George Loisos, "Effect of mechanical and Nd:YAG laser cutting on magnetic fluxdistribution near the cut edge of non-oriented steels," *Materials Processing Technology*, vol. 161, no. 1-2, pp. 151-155, 2005.

Valerii Abramenko received the Specialist degree in Electrical Drives and Automation of Industrial Installations from South Ural State University (SUSU), Chelyabinsk, Russia in 2014 and the Master of Science degree in Electrical Engineering jointly from SUSU and Lappeenranta University of Technology (LUT), Lappeenranta, Finland in 2017.

He is currently a researcher in the Department of Electrical Engineering, LUT. His research interests include high-efficient synchronous motors.

Jan Bárta received the B.Sc., M.Sc., and Ph.D. degrees in Power Electrical and Electronic Engineering from the Brno University of Technology, Brno, Czech Republic, in 2012, 2014 and 2018, respectively. He has been working as a member of Technical Staff with Brno University of Technology in research of electrical machines from 2014 to 2018. He is currently an Assistant Professor with the Department of Power Electrical and Electronic Engineering, Brno University of Technology. His research interest focuses on line-start synchronous machines, high-speed and high-efficiency electrical machines.

Iveta Lolová is Brno Ph.D. Talent Scholarship Holder – Funded by the Brno City Municipality. She received the B.Sc. and M.Sc. degrees in Power Electrical and Electronic Engineering from the Brno University of Technology, Brno, Czech Republic, in 2018 and 2020, respectively. She has been working as a Technical Staff with the Department of Power Electrical and Electronic Engineering in research of electrical machines since 2018. Her research interest focuses on line-start electrical machines and topology optimization of electrical machines.

Ilya Petrov received D.Sc. degree in 2015 from Lappeenranta University of Technology (LUT), Finland. He is currently a fellow researcher in the Department of Electrical Engineering, LUT.

Juha Pyrhönen (M'06–SM'18) born in 1957 in Kuusankoski, Finland, received the Doctor of Science (D.Sc.) degree from Lappeenranta University of Technology (LUT), Finland in 1991.

He became Professor of Electrical Machines and Drives in 1997 at LUT. He is engaged in research and development of electric motors and power-electronic-controlled drives. He has wide experience in the research and development of special electric drives for distributed power production, traction and high-speed applications. Permanent magnet materials and applying them in machines have an important role in his research. Currently, he is also researching new carbon-based materials for electrical machines.